

The ELM Survey. I. A Complete Sample of Extremely Low Mass White Dwarfs*

Warren R. Brown¹, Mukremin Kilic^{1,**}, Carlos Allende Prieto^{2,3}, and Scott J. Kenyon¹

¹*Smithsonian Astrophysical Observatory, 60 Garden St, Cambridge, MA 02138*

²*Instituto de Astrofísica de Canarias, E-38205, La Laguna, Tenerife, Spain*

³*Departamento de Astrofísica, Universidad de La Laguna, E-38205 La Laguna, Tenerife, Spain*

wbrown@cfa.harvard.edu, mkilic@cfa.harvard.edu, callende@iac.es,
skenyon@cfa.harvard.edu

ABSTRACT

We analyze radial velocity observations of the 12 extremely low-mass $\leq 0.25 M_{\odot}$ white dwarfs (WDs) in the MMT Hypervelocity Star Survey. Eleven of the 12 WDs are binaries with orbital periods shorter than 14 hours; the one non-variable WD is possibly a pole-on system among our non-kinematically selected targets. Our sample is unique: it is complete in a well-defined range of apparent magnitude and color. The orbital mass functions imply that the unseen companions are most likely other WDs, although neutron star companions cannot be excluded. Six of the 11 systems with orbital solutions will merge within a Hubble time due to the loss of angular momentum through gravitational wave radiation. The quickest merger is J0923+3028, a $g = 15.7$ ELM WD binary with a 1.08 hr orbital period and a ≤ 130 Myr merger time. The chance of a supernova Ia event among our ELM WDs is only 1% – 7%, however. Three binary systems (J0755+4906, J1233+1602, and J2119–0018) have extreme mass ratios and will most likely form stable mass-transfer AM CVn systems. Two of these objects, SDSS J1233+1602 and J2119–0018, are the lowest surface gravity WDs ever found; both show Ca II absorption likely from accretion of circumbinary material. We predict that at least one of our WDs is an eclipsing detached double WD system, important for constraining helium core WD models.

*Based on observations obtained at the MMT Observatory, a joint facility of the Smithsonian Institution and the University of Arizona.

** *Spitzer Fellow*

Subject headings: Galaxy: stellar content — stars: low-mass — stars: individual
 (SDSS J075552.40+490627.9, SDSS J081822.34+353618.9, SDSS J091709.55+463821.8,
 SDSS J092345.60+302805.0, SDSS J105353.89+520031.0, SDSS J123316.20+160204.6,
 SDSS J142200.74+435253.2, SDSS J143948.40+100221.7, SDSS J144801.13+134232.8,
 SDSS J151225.70+261538.5, SDSS J163026.09+271226.5, SDSS J211921.96–001825.8)
 — white dwarfs

1. INTRODUCTION

Extremely low mass (ELM) WDs, with masses $< 0.3 M_{\odot}$, are the remnants of stars that never ignited helium in their cores. The Universe is not old enough to produce ELM WDs by single star evolution. Thus ELM WDs must undergo significant mass loss during their evolution. Although metal-rich red giants with strong winds may evolve in isolation into single $\simeq 0.4 M_{\odot}$ WDs (Kilic et al. 2007c), producing $\simeq 0.2 M_{\odot}$ ELM WDs most likely requires compact binary systems (e.g. Marsh et al. 1995). Observational data for ELM WDs is limited, however, because of their rarity. For example, among the 9316 WDs identified in the Sloan Digital Sky Survey (SDSS), fewer than 0.2% have masses below $0.3 M_{\odot}$ (Eisenstein et al. 2006; Kepler et al. 2007).

Kilic et al. (2009, 2010b) have established a radial velocity program to search for companions around known ELM WDs. Of the six ELM WDs observed to date – including J0917+4638, the lowest mass WD known (Kilic et al. 2007b) – all six ELM WDs are in binaries with ≤ 1 day orbital periods. Two more recently identified ELM WDs, NLTT 11748 and J1257+5428 (Kawka & Vennes 2009; Marsh et al. 2010; Kulkarni & van Kerkwijk 2010), are also in binaries with < 1 day orbital periods (Steinfadt et al. 2010; Kawka et al. 2010; Kilic et al. 2010a). Three of these eight ELM WDs will merge due to gravitational wave radiation in less than 500 Myr (Mullally et al. 2009; Kilic et al. 2010b). A larger sample of ELM WDs is required to measure the space density, period distribution, and merger rate of these systems.

Here we present 12 ELM WDs with $\leq 0.25 M_{\odot}$ found in the Hypervelocity Star (HVS) Survey of Brown et al. (2005, 2006a,b, 2007a,b, 2009a,b), ten of which are new discoveries. Our ELM WD sample is unique because it comes from a complete, non-kinematically-selected survey of stars targeted in a well-defined range of apparent magnitude and color. Radial velocity follow-up reveals that 11 of the 12 ELM WDs are binaries with < 14 hr orbital periods. Clearly, the compact binary formation scenario is the best explanation for ELM

WDs.

In Section 2 we describe the survey design and the spectroscopic observations. In Section 3 we derive the physical parameters of the ELM WDs with stellar atmosphere modeling, and present the radial velocity curves for each object. In Section 4 we discuss the nature of the binary systems, and conclude in Section 5.

2. DATA

2.1. Survey Design

The ELM WDs reported here are found in the HVS survey, a radial velocity survey of objects with the colors of late-B type stars. All survey targets were selected from the Sloan Digital Sky Survey (SDSS) photometric catalog using de-reddened, uber-calibrated PSF magnitudes (Adelman-McCarthy et al. 2008). The HVS survey color selection is illustrated in Figure 1. Although the color selection was designed to exclude normal WDs by their $(u - g)$ color, the selection fortuitously includes low surface gravity WDs (see Figure 1).

The HVS survey consists of three parts. The first part of the HVS survey is defined by $15 < g_0 < 17$ (dash-dot line in Fig. 1) and is 100% complete over 7300 deg^2 of the SDSS Data Release 5 footprint Brown et al. (2007a). The second part of the HVS survey is defined by $17 < g_0 < 19.5$ (dashed line in Fig. 1) and is 100% complete over the same 7300 deg^2 of the SDSS Data Release 5 footprint Brown et al. (2007b). The final part extends the earlier surveys over 9800 deg^2 of the SDSS Data Release 7 footprint and also extends the magnitude limit to $g_0 = 20.5$ (dotted line), as described in Brown et al. (2009a). The final part of the HVS survey is currently 88% complete.

Our spectroscopy reveals that 15% of the HVS Survey targets are WDs. Two of the WDs with $\simeq 0.2 M_\odot$ are previously published elsewhere (Kilic et al. 2007a, 2010b). Here, we present the remaining ten WDs with mass $\leq 0.25 M_\odot$.

2.2. Spectroscopic Observations

With the exception of J0923+3028, we obtained all observations at the 6.5m MMT telescope using the Blue Channel spectrograph. We operate the spectrograph with the 832 line mm^{-1} grating in second order, providing wavelength coverage 3650 \AA to 4500 \AA and a spectral resolution of $1.0 - 1.2 \text{ \AA}$, depending on the slit size used. We obtain all observations at the parallactic angle, with a comparison lamp exposure paired with every observation.

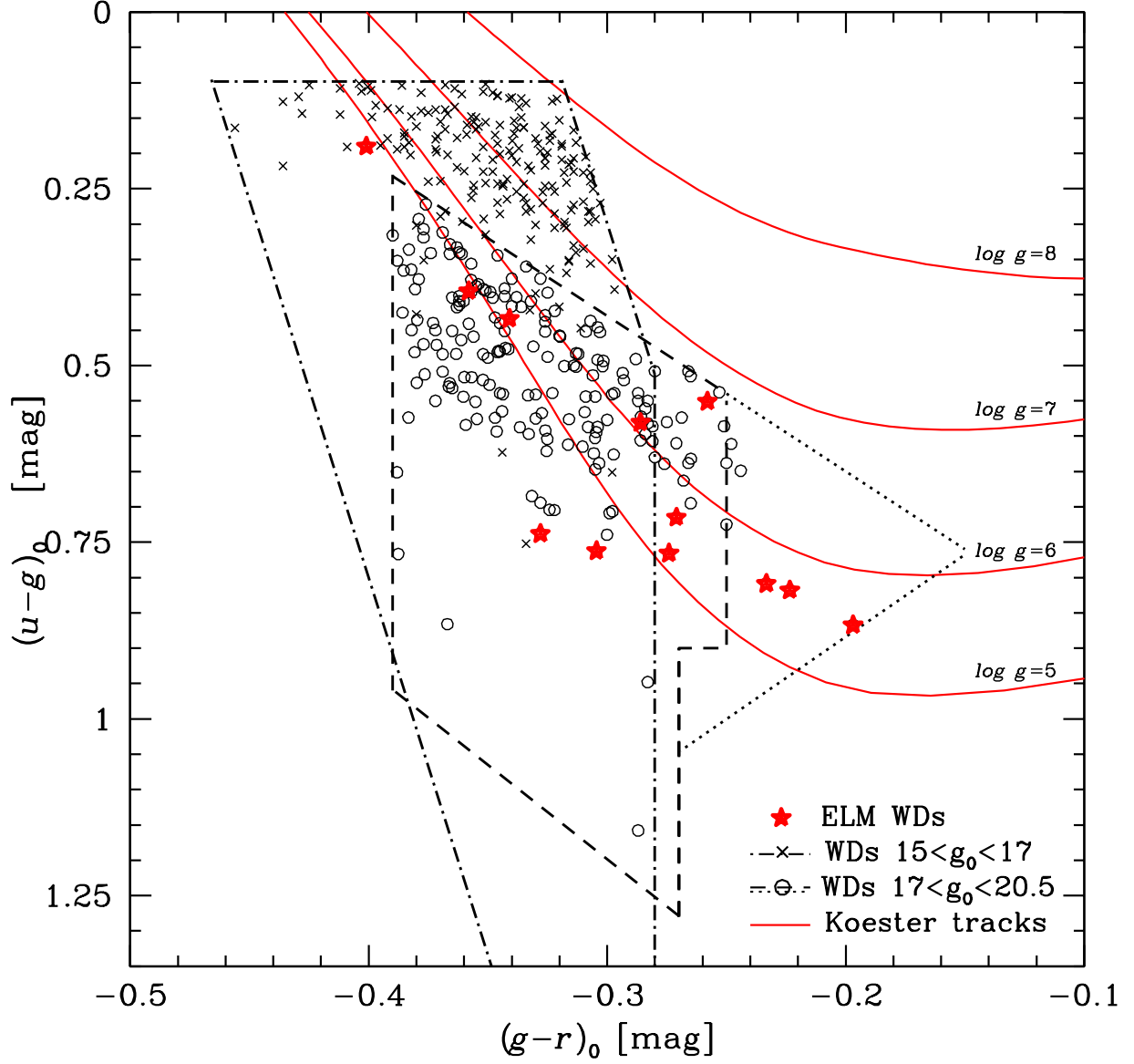


Fig. 1.— Color-color diagram showing the observed distribution of ELM WDs (*solid stars*) and the other WDs (*crosses, circles*) found in the HVS survey ($15 < g_0 < 17$ *dot-dash line*, $17 < g_0 < 19.5$ *dashed line*, $19.5 < g_0 < 20.5$ *dotted line*) compared with our synthetic photometry of the hydrogen atmosphere WD models of D. Koester (*solid lines*).

We obtained spectroscopy for J0923+3028 at the Fred Lawrence Whipple Observatory 1.5m Tillinghast telescope using the FAST spectrograph (Fabricant et al. 1998). We operate the FAST spectrograph with the 600 line mm^{-1} grating, providing wavelength coverage 3600 Å to 5500 Å and a spectral resolution of 2.3 Å. All observations are paired with a comparison lamp exposure.

We process the spectra using IRAF² in the standard way. We flux-calibrate using blue spectrophotometric standards (Massey et al. 1988), and we measure radial velocities using the cross-correlation package RVSAO (Kurtz & Mink 1998).

2.3. Radial Velocities

It is important to maximize velocity precision in our tests for variability, and we achieve the best precision by cross-correlating the ELM WDs with themselves. Our procedure begins by cross-correlating the observed spectra with a high signal-to-noise WD template to obtain preliminary velocities. We then shift the spectra to the rest frame, and sum them together to create templates for each target. Finally, we cross-correlate the spectra with the appropriate template to obtain the final velocities for each target. The average radial velocity uncertainty of the measurements is $\pm 18 \text{ km s}^{-1}$.

We check our velocities using WD model spectra with atmospheric parameters customized for each target. The results are consistent within 10 km s^{-1} , which we take as our systematic uncertainty. Table 3 in the Appendix presents the full set of radial velocity measurements for the 10 newly discovered ELM WDs presented here.

3. RESULTS

Our time-series spectroscopy provides for robust determinations of effective temperature and surface gravity for each object as well as its binary orbital parameters. Follow-up spectroscopy of J0917+4638 and J1053+5200 is already published (Kilic et al. 2007b, 2010b), but the other ELM WDs in our sample have not been studied until now.

²IRAF is distributed by the National Optical Astronomy Observatories, which are operated by the Association of Universities for Research in Astronomy, Inc., under cooperative agreement with the National Science Foundation.

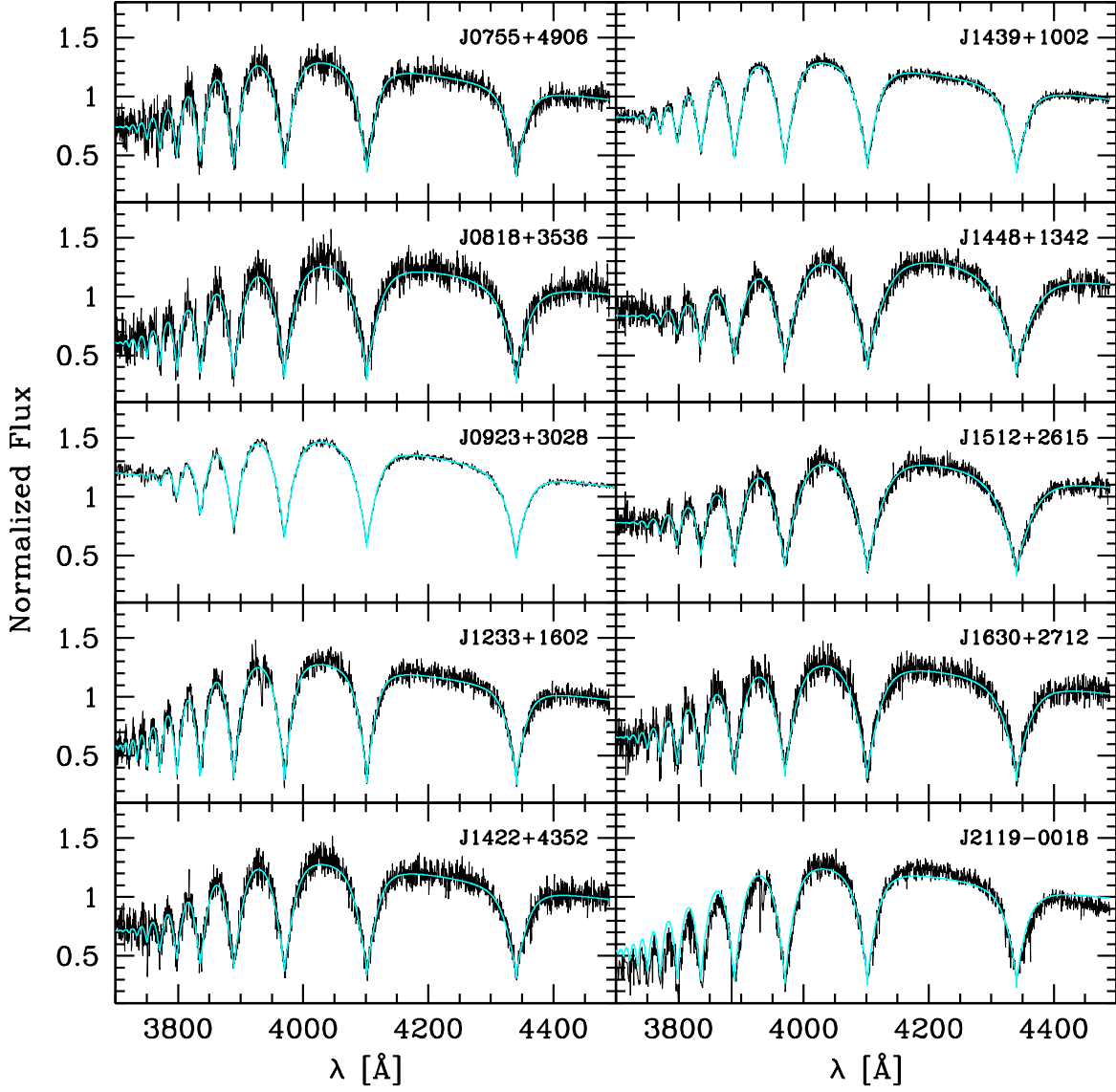


Fig. 2.— Model fits (*cyan lines*) overplotted on the composite observed spectra (*black lines*). The spectral continua provide improved T_{eff} determination except for the poorly fluxed-calibrated J2119–0018, for which we use the continuum-corrected spectrum.

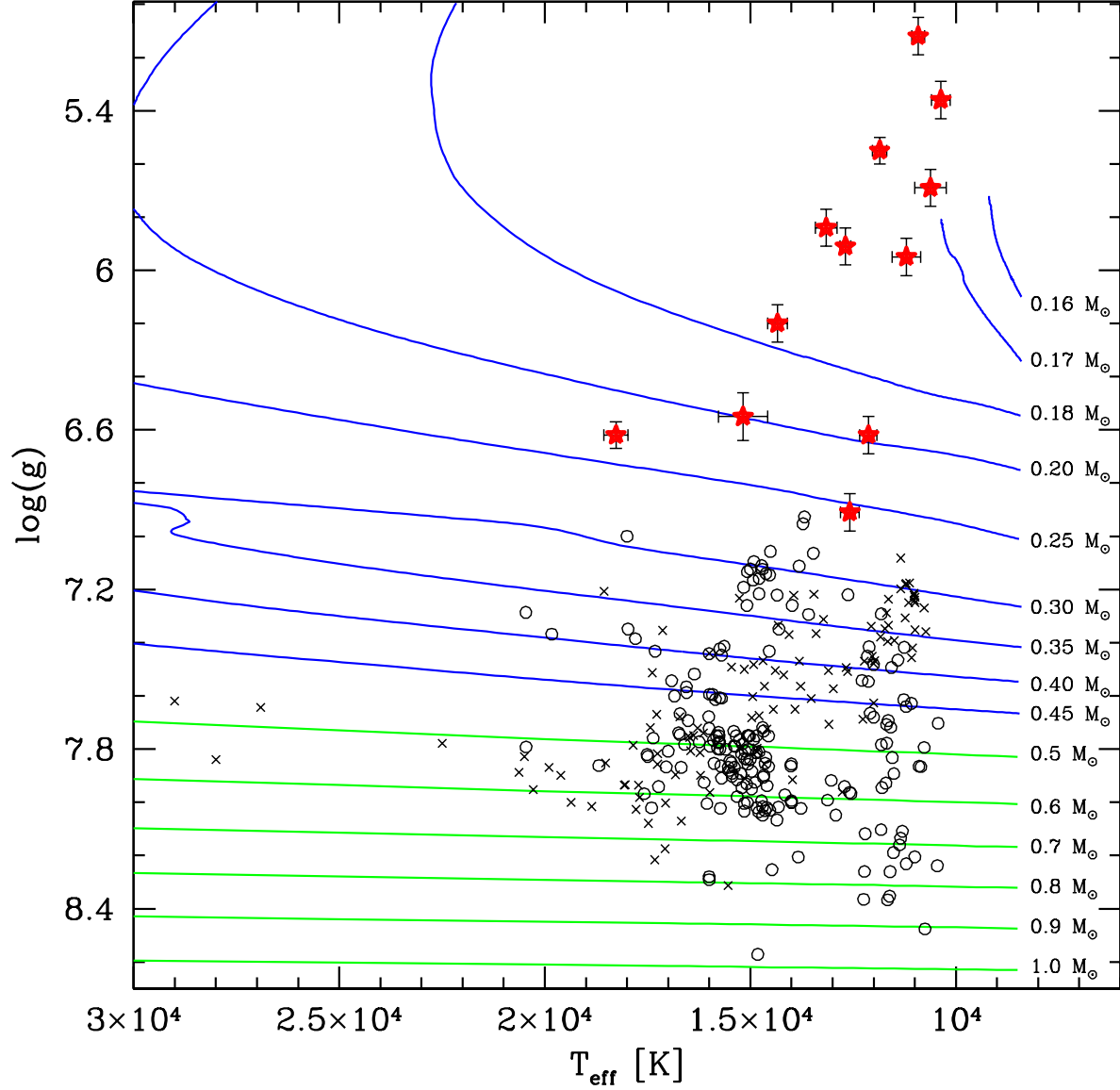


Fig. 3.— Surface gravity vs. effective temperature of the observed ELM WDs (*red stars*) and the other WDs (*crosses, circles*) found in the HVS survey, compared with predicted tracks for He WDs with $0.16\text{--}0.45\,M_{\odot}$ (*blue lines*, Panei et al. 2007) and CO WDs with $0.5\text{--}1.0\,M_{\odot}$ (*green lines*, Bergeron et al. 1995; Holberg & Bergeron 2006). Our sample of ELM WDs is defined by $m \leq 0.25\,M_{\odot}$.

3.1. Stellar Atmosphere Parameters

We perform stellar atmosphere model fits using synthetic DA WD spectra kindly provided by D. Koester. The grid of WD model atmospheres covers effective temperatures from 6000 K to 30,000 K in steps of 500 K to 2000 K, and surface gravities from $\log g = 5.0$ to 9.0 in steps of 0.25 dex. The model atmospheres are calculated assuming local thermodynamic equilibrium and include both convective and radiative transport (Koester 2008). We perform fits on the average composite spectra for each object and present the resulting T_{eff} and $\log g$ values in Table 1. We also perform fits to the individual spectra to derive a robust statistical error estimate for each object, also presented in Table 1. Figure 2 shows the composite spectra and our model fits. The surface gravities range 5.1–6.9 dex at effective temperatures of 10400–18300 K, confirming that the objects are ELM WDs.

We fit the flux-calibrated spectral continua to better measure effective temperature. The exception is J2119–0018, the one ELM WD we observed under variable conditions and at high airmass, for which we fit the continuum-corrected spectrum. If we fit only the continuum-corrected Balmer line profiles for all the ELM WDs, we obtain best-fit solutions that differ by 440 ± 190 K in T_{eff} and 0.04 ± 0.04 dex in $\log g$ from our published values. These differences reflect our systematic error, and demonstrate that our fits to the entire flux-calibrated spectra are reasonably accurate. Our fits also agree well with the SDSS photometry in all five filters, an additional demonstration that our temperature and surface gravity measurements are reliable.

Figure 3 compares the observed ELM WDs and other WDs in the HVS survey with the improved Panei et al. (2007) tracks (see Kilic et al. 2010b) for He-core WDs with masses 0.16–0.45 M_{\odot} and the Bergeron et al. (1995)³ tracks for normal CO-core WDs with masses 0.5–1 M_{\odot} . The gap between the 0.17 M_{\odot} and 0.18 M_{\odot} He-core WD tracks is linked to the threshold for thermonuclear flashes in the hydrogen shell burning phase (Panei et al. 2007). Remarkably, the majority of observed ELM WDs fall in the gap of parameter space between the 0.17 M_{\odot} and 0.18 M_{\odot} models.

The inconsistency between the observations and the He-core WD models make accurate mass and luminosity estimates difficult. Fortunately, mass and luminosity change slowly over the range of effective temperature and surface gravity sampled by our ELM WDs. We conclude that the majority of the ELM WDs have a mass of $\simeq 0.17 M_{\odot}$ and an absolute magnitudes of $M_g \simeq 8$; more precise estimates are possible for the 0.20 - 0.25 M_{\odot} ELM WDs and are summarized in Table 1.

³<http://www.astro.umontreal.ca/~bergeron/CoolingModels/>

Using these absolute magnitude estimates, the majority of our ELM WDs are found at heliocentric distances of $1 < d < 3$ kpc. The notable exception is J0923+3028, a bright $g = 15.7$ ELM WD approximately 280 pc distant. All of our ELM WDs are located at high Galactic latitudes $30^\circ < |b| < 80^\circ$ in the SDSS imaging footprint.

The systemic velocities suggest that two objects are halo WDs: J0818+3536 and J1422+4352 have systemic heliocentric radial velocities of -201 ± 4 km s $^{-1}$ and -195 ± 8 km s $^{-1}$, respectively. Kilic et al. (2010b) also identify J1053+5200 as a halo object based on its proper motion and distance estimate. Unfortunately, reliable proper motions are unavailable for our fainter $g \simeq 20$ WDs. Despite having relatively large > 1 kpc distances above the Galactic plane, the remaining ELM WDs in our sample have systemic radial velocities consistent with a disk origin.

3.2. Orbital Parameters

Eleven of our twelve ELM WDs exhibit significant radial velocity variation, with peak-to-peak velocity amplitudes up to 890 km s $^{-1}$. We compute orbital periods for these systems by finding the period that minimizes χ^2 for a circular orbit. Figure 4 plots the periodograms for the 10 new ELM WDs. A few ELM WDs have multiple period solutions because of insufficient coverage, however in all cases the periods are constrained to be < 1 day. We estimate the period error by conservatively identifying the range of periods with $\chi^2 \leq 2\chi_{\min}^2$, where χ_{\min}^2 is the minimum χ^2 .

We compute best-fit orbital elements using the code of Kenyon & Garcia (1986), which weights each velocity measurement by its associated error. The uncertainties in the orbital elements are derived from the covariance matrix and χ^2 . To verify these uncertainty estimates, we perform a Monte Carlo analysis where we replace the measured radial velocity v with $v + g\delta v$, where δv is the error in v and g is a Gaussian deviate with zero mean and unit variance. For each of 10000 sets of modified radial velocities, we repeat the periodogram analysis and derive new orbital elements. We adopt the inter-quartile range in the period and orbital elements as the uncertainty. For binaries with multiple period aliases, both approaches yield similar uncertainties. When there are several equally plausible periods, the Monte Carlo analysis selects all possible periods and derives very large uncertainties. In these cases, we adopt errors from the covariance matrix for the lowest χ^2 orbital period.

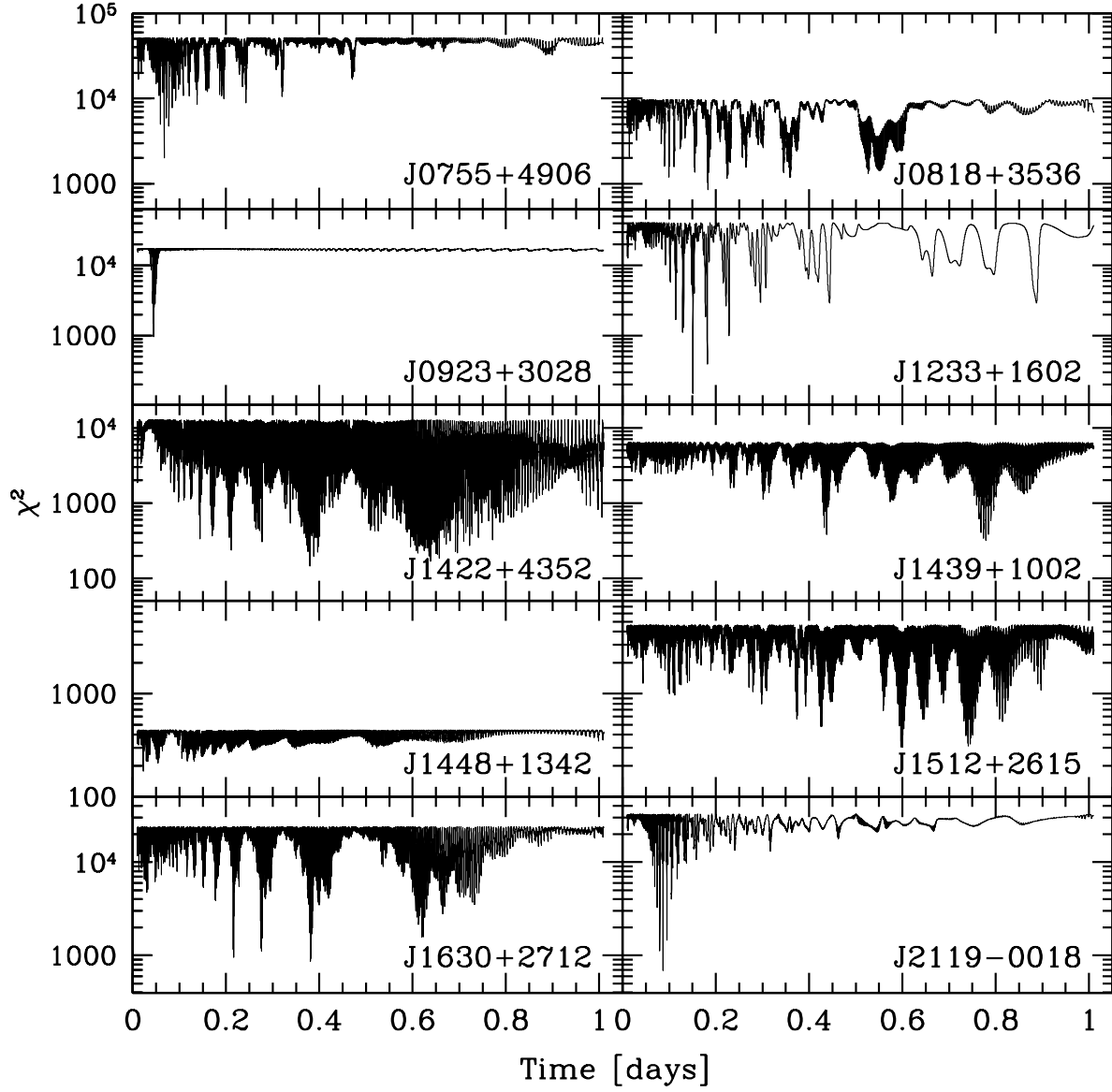


Fig. 4.— Periodograms for the 10 new ELM WDs. Some objects have multiple period aliases because of insufficient coverage, however in all cases the periods are constrained to <1 day. J1448+1342 is formally consistent with no velocity variability.

Table 1. White Dwarf Physical Parameters

Object	g_0 (mag)	$(u - g)_0$ (mag)	$(g - r)_0$ (mag)	T_{eff} (K)	$\log g$	M_g (mag)	d_{helio} (kpc)	Mass (M_{\odot})
J0755+4906	20.095 ± 0.023	0.763 ± 0.086	-0.304 ± 0.039	13160 ± 260	5.84 ± 0.07	8.0	2.62	0.17
J0818+3536	20.484 ± 0.030	0.766 ± 0.152	-0.274 ± 0.058	10620 ± 380	5.69 ± 0.07	8.0	3.14	0.17
J0917+4638 ¹	18.696 ± 0.019	0.738 ± 0.037	-0.328 ± 0.024	11850 ± 170	5.55 ± 0.05	8.0	1.38	0.17
J0923+3028	15.628 ± 0.018	0.190 ± 0.027	-0.401 ± 0.021	18350 ± 290	6.63 ± 0.05	8.4	0.28	0.23
J1053+5200 ²	18.874 ± 0.023	0.395 ± 0.049	-0.358 ± 0.045	15180 ± 600	6.55 ± 0.09	8.7	1.08	0.20
J1233+1602	19.829 ± 0.018	0.809 ± 0.068	-0.233 ± 0.028	10920 ± 160	5.12 ± 0.07	8.0	2.32	0.17
J1422+4352	19.794 ± 0.020	0.715 ± 0.061	-0.271 ± 0.032	12690 ± 130	5.91 ± 0.07	8.0	2.29	0.17
J1439+1002	17.812 ± 0.016	0.434 ± 0.042	-0.341 ± 0.026	14340 ± 240	6.20 ± 0.07	8.0	0.92	0.18
J1448+1342	19.217 ± 0.023	0.581 ± 0.047	-0.286 ± 0.033	12580 ± 230	6.91 ± 0.07	9.9	0.73	0.25
J1512+2615	19.241 ± 0.021	0.551 ± 0.051	-0.258 ± 0.030	12130 ± 210	6.62 ± 0.07	9.3	0.97	0.20
J1630+2712	20.040 ± 0.019	0.818 ± 0.083	-0.223 ± 0.031	11200 ± 350	5.95 ± 0.07	8.0	2.56	0.17
J2119–0018	20.000 ± 0.021	0.867 ± 0.092	-0.197 ± 0.033	10360 ± 230	5.36 ± 0.07	8.0	2.51	0.17

References. — ¹ Kilic et al. (2007b); ² Kilic et al. (2010b)

Table 2. Binary Orbital Parameters

Object	P (days)	K (km s ⁻¹)	V_{systemic} (km s ⁻¹)	Spec. Conjunction (days + 2450000)	Mass Function	M_2 (M _⊙)	τ_{merge} (Gyr)
J0755+4906	0.06302 ± 0.00213	438 ± 5	-51 ± 4	5150.84949 ± 0.00010	0.550 ± 0.025	≥ 0.81	≤ 0.22
J0818+3536	0.18315 ± 0.02110	170 ± 5	-201 ± 4	5151.90466 ± 0.00030	0.094 ± 0.014	≥ 0.26	≤ 8.89
J0917+4638 ¹	0.31642 ± 0.00002	145 ± 2	28 ± 1	3708.85755 ± 0.00134	0.102 ± 0.003	≥ 0.27	≤ 36.8
J0923+3028	0.04495 ± 0.00049	296 ± 3	2 ± 2	3818.67019 ± 0.00002	0.121 ± 0.004	≥ 0.34	≤ 0.13
J1053+5200 ²	0.04256 ± 0.00002	264 ± 2	12 ± 2	3790.79731 ± 0.00004	0.081 ± 0.002	≥ 0.26	≤ 0.16
J1233+1602	0.15090 ± 0.00009	336 ± 4	-35 ± 3	5268.84901 ± 0.00014	0.597 ± 0.020	≥ 0.86	≤ 2.14
J1422+4352	0.37930 ± 0.01123	176 ± 6	-195 ± 8	4596.92484 ± 0.00068	0.208 ± 0.023	≥ 0.41	≤ 42.9
J1439+1002	0.43741 ± 0.00169	174 ± 2	-55 ± 1	3882.68848 ± 0.00079	0.240 ± 0.007	≥ 0.46	≤ 54.7
J1448+1342 ³	...	35 ± 7	-28 ± 5
J1512+2615	0.59999 ± 0.02348	115 ± 4	-41 ± 4	3879.48768 ± 0.00119	0.097 ± 0.012	≥ 0.28	≤ 171
J1630+2712	0.27646 ± 0.00002	218 ± 5	-118 ± 3	5009.72779 ± 0.00016	0.295 ± 0.018	≥ 0.52	≤ 15.6
J2119-0018	0.08677 ± 0.00004	383 ± 4	-28 ± 4	5008.88701 ± 0.00003	0.501 ± 0.016	≥ 0.75	≤ 0.54

References. — ¹ Kilic et al. (2007b); ² Kilic et al. (2010b)

Note. — ³ The measurements are formally consistent with no variation.

We present the best-fit orbital parameters in Table 2. Columns include orbital period (P), radial velocity semi-amplitude (K), systemic velocity (V_{systemic}), the time of spectroscopic conjunction (the time when the object passes through 0 km s^{-1} as it approaches the observer), mass function (see Eqn. 1 below), and minimum secondary mass (assuming $i = 90^\circ$). The systemic velocities in Table 2 are not corrected for the WDs’ gravitational redshifts, which should be subtracted from the observed velocities to find the true systemic velocities. This correction is approximately 3 km s^{-1} for our targets.

We plot the best-fit orbits compared to the observed radial velocities in Figure 5, excluding the two objects previously published. Follow-up observations were typically obtained over a pair of 3-day time baselines separated by one week, plus an original observation that extends the baseline up to 1488 days (not shown in the upper panel of Fig. 5). The ELM WD’s short orbital periods combined with our long time baselines allow us to constrain the orbital periods accurately.

4. DISCUSSION

4.1. J0755+4906

SDSS J075552.40+490627.9 exhibits the largest radial velocity variation in our sample of ELM WDs. The WD has a best-fit amplitude of $876 \pm 10 \text{ km s}^{-1}$, an orbital period of $1.512 \pm 0.051 \text{ hr}$, and a binary mass function of

$$\frac{M_2^3 \sin^3 i}{(M_1 + M_2)^2} = \frac{PK^3}{2\pi G} = 0.550 \pm 0.025 M_\odot, \quad (1)$$

where i is the orbital inclination angle, M_1 is the ELM WD mass, and M_2 is the companion mass. Although the inclination is unknown, we can use the distribution of possible inclinations to constrain the companion’s mass.

Given the observed orbital parameters, there is a 61% probability that J0755+4906’s companion is a WD with $<1.4 M_\odot$ and a 20% probability that the companion is a neutron star with $1.4\text{--}3.0 M_\odot$. The remaining probability is for a companion mass $>3 M_\odot$. We estimate the most probable companion mass by assuming the mean inclination angle for a random stellar sample, $i = 60^\circ$. For J0755+4906, the most likely companion is a $1.12 M_\odot$ object at an orbital separation of $0.7 R_\odot$. Follow-up radio or X-ray observations are required to rule out a neutron star companion, but statistically the companion is most likely a massive WD.

Short period binaries like J0755+4906 must eventually merge due to angular momentum

loss to gravitational wave radiation. The merger time is

$$\tau = \frac{(M_1 + M_2)^{1/3}}{M_1 M_2} P^{8/3} \times 10^{-2} \text{Gyr} \quad (2)$$

where the masses are in M_\odot and the period P is in hours (Landau & Lifshitz 1958). For a companion mass of $1.1 M_\odot$, J0755+4906 will merge in 170 Myr. Kilic et al. (2010b) discuss the many possible stellar evolution paths for such a merging system. For J0755+4906, there is at least a 6% likelihood that the system contains a pair of WDs whose total mass exceeds the Chandrasekhar mass and thus will explode as a Type Ia supernova. On the other hand, the extreme mass ratio $M_1/M_2 \leq 0.21$ means that mass transfer is likely to be stable and thus this binary will probably evolve into an AM CVn system.

4.2. J0818+3536

The best-fit orbital period for SDSS J081822.34+353618.9 is 4.396 ± 0.51 hr, however the limited number of follow-up observations allow for aliases at 5.4 and 8.6 hr periods. Periods longer than 14 hr are ruled out. Thus J0818+3536 is a short period binary. Assuming the best-fit period, there is a 90% probability that the companion is a WD with $< 1.4 M_\odot$ and a 5% probability that the companion is a neutron star with $1.4\text{--}3.0 M_\odot$. For the most probable inclination angle $i = 60^\circ$, the companion is a $0.33 M_\odot$ low mass WD at orbital separation of $1.1 R_\odot$.

4.3. J0917+4638

Previously published by Kilic et al. (2007b), SDSS J091709.55+463821.8 has a binary orbital period of 7.5936 ± 0.0005 hr. Assuming an inclination angle of 60° , its companion is another low-mass WD with $0.35 M_\odot$ at an orbital separation of $1.6 R_\odot$.

Curiously, J0917+4638 and the two other ELM WDs with lower surface gravity in our sample (J1233+1602 and J2119–0018) all show significant Ca II K absorption in their atmospheres (Figure 2). The extremely short timescale for gravitational settling of Ca in the WD photospheres means there must be an external source for the observed metals (Koester & Wilken 2006; Kilic et al. 2007a). The ELM WDs are located far above the Galactic plane where accretion from the interstellar medium is unlikely. A plausible source of Ca is accretion from a circumbinary disk created during the mass loss phase of the giant. Since the ELM WDs all went through a common envelope phase with a companion, a left-over circumbinary disk is possible.

4.4. J0923+3028

SDSS J092345.60+302805.0 is the brightest ELM WD in our sample, with $g = 15.7$ mag and a heliocentric distance estimate of 280 pc. J0923+3028 has a binary orbital period of 1.079 ± 0.012 hr and a mass function of $0.121 \pm 0.004 M_{\odot}$. There is a 87% probability that the companion is a WD with $< 1.4 M_{\odot}$ and a 6% probability that the companion is a neutron star with $1.4\text{--}3.0 M_{\odot}$. For the most probable inclination angle, $i = 60^{\circ}$, the companion is a $0.44 M_{\odot}$ WD at orbital separation of $0.5 R_{\odot}$. Thus, J0923+3028 is the second shortest period double WD system after J1053+5200 (Kilic et al. 2010b). This system will merge in less than 130 Myr.

J0923+3028 is the one ELM WD in our sample with a significant proper motion measurement, $\mu_{\alpha} \cos \delta = -4.2 \pm 3.5$ and $\mu_{\delta} = -25 \pm 3.5$ mas yr $^{-1}$ (Munn et al. 2004). The gravitational redshift of the WD is $\simeq 4$ km s $^{-1}$, thus its true systemic velocity is -2 ± 5 km s $^{-1}$. The velocity components with respect to the local standard of rest (Schönrich et al. 2010) are $U = 14 \pm 6$, $V = -20 \pm 8$, $W = -2 \pm 6$ km s $^{-1}$. J0923+3028 is clearly a disk star.

4.5. J1053+5200

Previously published by Kilic et al. (2010b), SDSS J105353.89+520031.0 has a binary orbital period of 1.0224 ± 0.0005 hr. Assuming an inclination angle of 60° , the companion is another low mass WD with $0.33 M_{\odot}$ at an orbital separation of $0.4 R_{\odot}$. This system will merge in less than 160 Myr.

4.6. J1233+1602

SDSS J123316.20+160204.6 is the lowest surface gravity WD known. Its surface gravity, $\log g = 5.12 \pm 0.07$, is comparable to a $2.5 M_{\odot}$ main sequence star with $\log g \simeq 4.2$ (Girardi et al. 2002, 2004). However, J1233+1602’s binary orbital parameters exclude the possibility of it being a main sequence star.

J1233+1602 is a binary with a 3.6216 ± 0.0022 hr orbital period and a mass function of $0.597 \pm 0.020 M_{\odot}$. By assuming an edge-on orbit, $i = 90^{\circ}$, we can place a lower limit on the companion mass. For a $2.5 M_{\odot}$ A star primary, the star must have at least a $2.44 M_{\odot}$ companion at an orbital separation of $2.0 R_{\odot}$. However, the radius of a $2.5 M_{\odot}$ main sequence star is $1.9 R_{\odot}$. Thus the orbital separation of two A stars in this system is less than their summed radii. Even if the companion were a $2.44 M_{\odot}$ neutron star, the system

would still be in Roche-lobe overflow, for which we see no evidence.

As a check, we combine the spectra near maximum blue-shift and red-shift into two composite spectra. If there is a contribution from the companion, it may be visible as second pair of lines or an asymmetry in the line profiles. We do not see any extra lines or asymmetries in the line profiles. We conclude J1233+1602 is a $\simeq 0.17 M_{\odot}$ WD orbiting a much fainter companion.

Given the observed mass function, there is a 58% probability that the companion is a WD with $< 1.4 M_{\odot}$ and a 21% probability that the companion is a neutron star with $1.4\text{--}3.0 M_{\odot}$. Assuming the most probable orbital inclination angle of 60° , J1233+1602’s companion is a $1.2 M_{\odot}$ WD at an orbital separation of $1.3 R_{\odot}$. Follow-up radio or X-ray observations are required to rule out a neutron star companion, but statistically the companion is most likely a massive WD.

There is a 7% likelihood that this system contains a pair of WDs whose total mass exceeds the Chandrasekhar mass and thus will explode as a Type Ia supernova. The merger time for such a system is < 2 Gyr. However, the extreme mass ratio $M_1/M_2 \leq 0.20$ suggests that mass transfer will be stable and this binary will likely evolve into an AM CVn system.

4.7. J1422+4352

SDSS J142200.74+435253.2 has the fewest follow-up observations yet its binary orbital period is reasonably well constrained. The best-fit period is 9.10 ± 0.27 hrs, with a significant alias at 15.3 hrs. Assuming the best-fit period, there is a 82% probability that the companion is a WD with $< 1.4 M_{\odot}$ and a 8% probability that the companion is a neutron star with $1.4\text{--}3.0 M_{\odot}$. For the most probable inclination angle, $i = 60^{\circ}$, the companion is a normal $0.55 M_{\odot}$ WD at orbital separation of $2.0 R_{\odot}$.

4.8. J1439+1002

SDSS J143948.40+100221.7 is a binary with a best-fit period of 10.498 ± 0.041 hrs. Despite having follow-up observations on 10 nights spaced over one year (see Fig. 5) there remains a significant period alias at 18.576 ± 0.215 hr. Using the best-fit orbital solution, there is a 80% probability that the companion is a WD with $< 1.4 M_{\odot}$ and a 10% probability that the companion is a neutron star with $1.4\text{--}3.0 M_{\odot}$. For the most probable inclination angle, $i = 60^{\circ}$, the companion is a normal $0.62 M_{\odot}$ WD at orbital separation of $2.2 R_{\odot}$.

4.9. J1448+1342

SDSS J144801.13+134232.8 is the one ELM WD for which we detect no significant velocity variation. The best-fit orbit (0.5 hr period) has a reduced χ^2 identical to a constant-velocity fit, thus this system can have a velocity semi-amplitude no larger than $K \leq 35 \pm 11$ km s⁻¹. By comparison, the average semi-amplitude of the other eleven ELM WD binaries is 240 km s⁻¹. The required orbital inclination for J1448+1342 to have the average semi-amplitude of the other ELM WD binaries is $i \leq 8^\circ$.

J1448+1342 may be either a pole-on binary system or a single star. If the orbital inclinations of our non-kinematically selected ELM WDs are randomly distributed, we expect one of the twelve ELM WDs to have $i \leq 23.5^\circ$; there is a 12% likelihood of finding one of the twelve systems with $i \leq 8^\circ$. Thus it is possible that J1448+1342 is a pole-on binary system. The alternative is that J1448+1342 is a single star. It is intriguing that J1448+1342 is the most massive object in our sample of 12 ELM WDs. Existing stellar evolution models, however, cannot explain 0.25 M_⊙ WDs from single star evolution, even with extreme mass loss models (Kilic et al. 2007c). Additional observations are required to determine the nature of this ELM WD.

4.10. J1512+2615

SDSS J151225.70+261538.5 is a binary with a best-fit orbital period of 14.40 ± 0.56 hr, and a significant period alias at 17.8 hrs. Assuming the best-fit period, there is an 89% probability that the companion is a WD with <1.4 M_⊙ and a 5% probability that the companion is a neutron star with 1.4-3.0 M_⊙. For the most probable inclination angle $i = 60^\circ$, the companion is a 0.36 M_⊙ low mass WD at orbital separation of 2.5 R_⊙.

4.11. J1630+2712

SDSS J163026.09+271226.5 has a best-fit orbital period of 6.6350 ± 0.0005 hr. The observations also allow for 5.16 and 9.17 hr periods. Assuming the best-fit period, there is a 77% probability that the companion is a WD with <1.4 M_⊙ and a 11% probability that the companion is a neutron star with 1.4-3.0 M_⊙. For the most probable inclination angle $i = 60^\circ$, the companion is a normal 0.70 M_⊙ WD at an orbital separation of 1.7 R_⊙.

4.12. J2119–0018

SDSS J211921.96–001825.8 is the second lowest surface gravity WD known, with $\log g = 5.36 \pm 0.07$. As with J1233+1602, J2119–0018’s orbital parameters exclude the possibility of it being a main sequence A star.

J2119–0018 is a binary with a 2.0825 ± 0.0010 hr orbital period and a mass function of $0.501 \pm 0.016 M_{\odot}$. If the primary is $2.5 M_{\odot}$ main sequence star, its companion must be $\geq 2.2 M_{\odot}$ at an orbital separation of $1.4 R_{\odot}$. This separation is smaller than the radius of main sequence stars. We do not see any evidence of a companion in our spectra. Thus J2119–0018 must be a $\simeq 0.17 M_{\odot}$ WD.

Given the observed orbital parameters, there is a 64% probability that the companion is a WD with $< 1.4 M_{\odot}$ and a 18% probability that the companion is a neutron star with $1.4\text{--}3.0 M_{\odot}$. Assuming the most probable orbital inclination angle of 60° , J2119–0018’s companion is a $1.04 M_{\odot}$ WD at an orbital separation of $0.9 R_{\odot}$. Follow-up radio or X-ray observations are required to rule out a neutron star companion, but the companion is most likely a massive WD.

This system will merge in less than 540 Myr. There is a 5% likelihood that the system contains a pair of WDs whose total mass exceeds the Chandrasekhar mass and thus will explode as a Type Ia supernova. However, the extreme mass ratio $M_1/M_2 \leq 0.23$ suggests that mass transfer will be stable and this binary will likely evolve into an AM CVn system.

5. CONCLUSION

We present a complete sample of 12 ELM WDs with masses $\leq 0.25 M_{\odot}$ in the HVS Survey. Eleven of the WDs are binary systems with orbital periods < 14 hr; J1448+1342 is the only WD for which we detect no velocity variation. Given the binary nature of the other WDs in our non-kinematically selected sample, J1448+1342 is quite possibly a pole-on system. Our observations demonstrate that the formation of $\leq 0.25 M_{\odot}$ ELM WDs requires close binary evolution (Marsh et al. 1995).

Two of our targets, J1233+1602 and J2119–0018, have surface gravities lower than the previous record-holder J0917+4638 (Kilic et al. 2007a) and thus are the lowest surface gravity WDs currently known. Interestingly, all three of these low surface gravity ELM WDs exhibit strong Ca absorption in their spectra. The Ca is likely explained by on-going accretion from circumbinary disks. Other sources of accretion are much less likely, given the extremely short timescale for gravitational settling in the ELM WD photospheres and their

1-2 kpc distances above the disk plane.

One possible source of circumbinary disk accretion is debris from former planetary systems (Dong et al. 2010). For the case of our ELM WD binaries, the systems must have had circumbinary planets that could survive the binary common envelope evolution. Common envelope evolution may also lead to “second generation” planet formation (Perets 2010), the debris of which may be accreting onto the ELM WDs. In any case, the lowest surface gravity ELM WDs are interesting targets for future infrared observations.

Six of our 12 ELM WDs (50%) will merge within a Hubble time (we exclude J1448+1342 due to its unknown period); four of these mergers will happen in ≤ 600 Myr. In all cases the most likely binary companions are WDs, although neutron stars cannot be ruled out based on the available data. Two of the merger systems, J0818+3536 and J1053+5200, are likely to have unusually low-mass ($< 0.4 M_{\odot}$) WD companions and thus are possible progenitors for single helium-enriched sdO stars (Heber 2009). Four of the merger systems are likely to have C/O WD companions and thus will likely form extreme helium stars. However, three of the systems (J0755+4906, J1233+1602, and J2119–0018) have such extreme mass ratios ≤ 0.23 that future mass transfer is likely to be stable and thus they will evolve into AM CVn systems.

We expect that at least one of our ELM WDs has $i > 85^{\circ}$ and thus is an eclipsing system. Steinfadt et al. (2010) recently discovered the first eclipsing detached double WD; finding eclipsing WD binaries in our sample will provide important mass-radius constraints on He core ELM WD models. The most probable eclipsing candidates in our sample are the systems with the shortest merger times, namely J0923+3028, J1053+5200, J0755+4906, and J2119–0018.

Our sample of 12 ELM WDs is unique in terms of its non-kinematic selection and its completeness. Previous discoveries of ELM WDs in the SDSS (Liebert et al. 2004; Eisenstein et al. 2006) and other surveys (Kawka et al. 2006; Kawka & Vennes 2009) have been useful for studying the formation and future evolution of the individual systems (Kilic et al. 2010b). However, the spectroscopic selection biases present in the SDSS prohibit an accurate estimate of the space density of these objects. SDSS WDs were observed by different targeting programs selected with different color, magnitude, and photometric quality cuts as well as different sparse sampling rates that vary over the SDSS survey region (Eisenstein et al. 2006). Our sample, on the other hand, is complete in magnitude, color, and spatial coverage and enables us to estimate the space density and merger rate of ELM WDs in the Milky Way. We explore possible links to underluminous supernovae, AM CVn stars, and other phenomena in a companion paper (Brown et al. 2010).

We thank M. Alegria, J. McAfee, and A. Milone for their assistance with observations obtained at the MMT Observatory, and P. Berlind and M. Calkins for their assistance with observations obtained at the Fred Lawrence Whipple Observatory. We especially thank P. Challis obtaining additional observations of J2119–0018, and the referee for helpful comments. This project makes use of data products from the Sloan Digital Sky Survey, which is managed by the Astrophysical Research Consortium for the Participating Institutions. This research makes use of NASA’s Astrophysics Data System Bibliographic Services. To perform the Monte Carlo analysis, we used the routine `randgen.f`, written by R. Chandler and P. Northrop. This work was supported in part by the Smithsonian Institution. MK is supported by NASA through the *Spitzer Space Telescope* Fellowship Program, under an award from CalTech.

Facilities: MMT (Blue Channel Spectrograph)

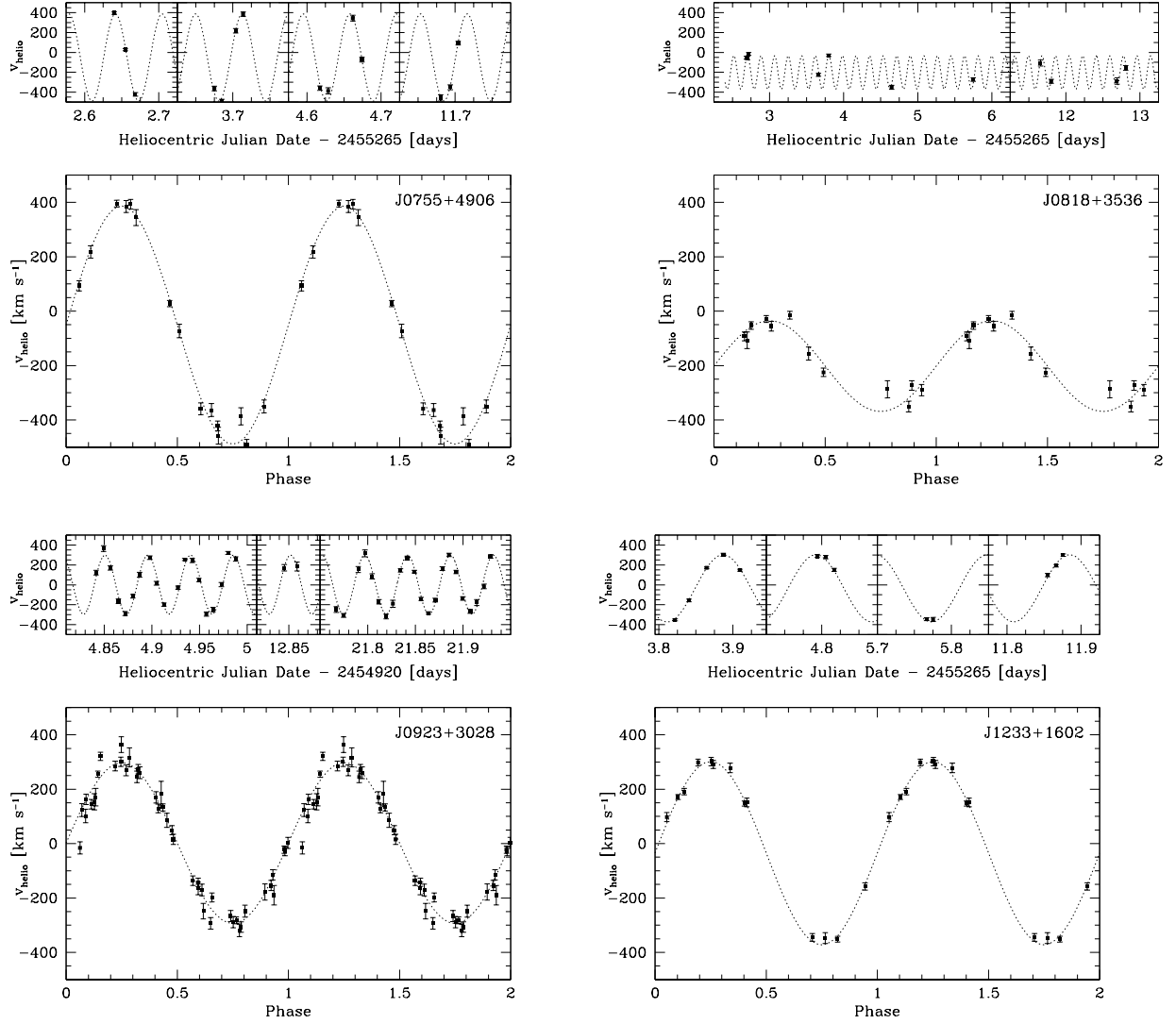


Fig. 5.— Data and best-fit orbits for the 10 new ELM WDs. Upper panels plot the heliocentric radial velocities vs. time. Lower panels plot the observations phased to the best-fit orbital solution (Table 2), and also include the observation first used to identify the ELM WD candidate. The same vertical axis is used in all 10 plots.

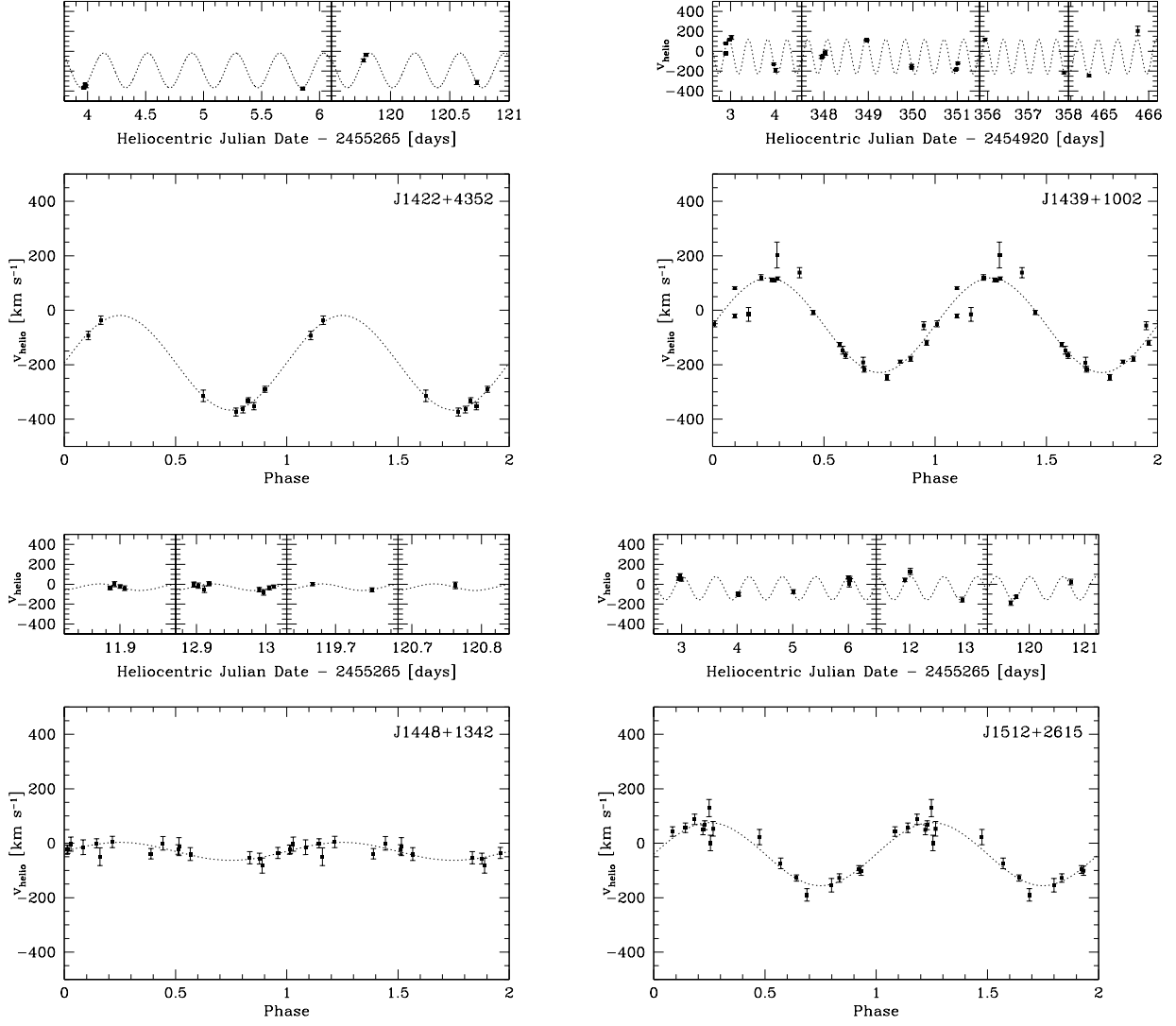


Fig. 5.— Continued

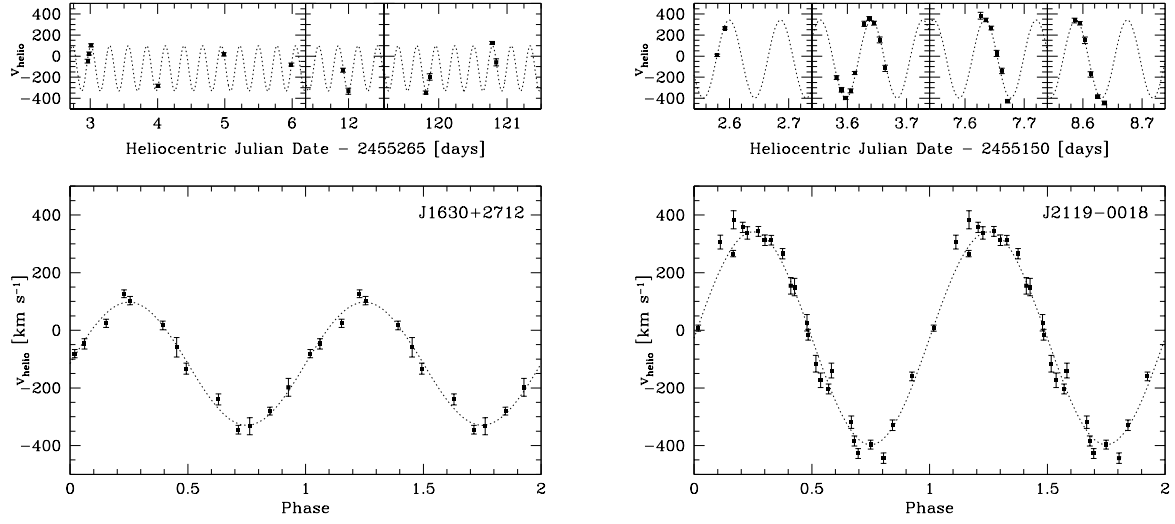


Fig. 5.— Continued

REFERENCES

- Adelman-McCarthy, J. K. et al. 2008, *ApJS*, 175, 297
- Bergeron, P., Wesemael, F., & Beauchamp, A. 1995, *PASP*, 107, 1047
- Brown, W. R., Geller, M. J., & Kenyon, S. J. 2009a, *ApJ*, 690, 1639
- Brown, W. R., Geller, M. J., Kenyon, S. J., & Bromley, B. C. 2009b, *ApJ*, 690, L69
- Brown, W. R., Geller, M. J., Kenyon, S. J., & Kurtz, M. J. 2005, *ApJ*, 622, L33
- . 2006a, *ApJ*, 640, L35
- . 2006b, *ApJ*, 647, 303
- Brown, W. R., Geller, M. J., Kenyon, S. J., Kurtz, M. J., & Bromley, B. C. 2007a, *ApJ*, 660, 311
- . 2007b, *ApJ*, 671, 1708
- Brown, W. R., Kilic, M., Allende Prieto, C., & Kenyon, S. J. 2010, *MNRAS*, submitted
- Dong, R., Wang, Y., Lin, D. N. C., & Liu, X. 2010, *ApJ*, 715, 1036
- Eisenstein, D. J. et al. 2006, *ApJS*, 167, 40
- Fabricant, D., Cheimets, P., Caldwell, N., & Geary, J. 1998, *PASP*, 110, 79
- Girardi, L., Grebel, E. K., Odenkirchen, M., & Chiosi, C. 2004, *A&A*, 422, 205
- Girardi, L. et al. 2002, *A&A*, 391, 195
- Heber, U. 2009, *ARA&A*, 47, 211
- Holberg, J. B. & Bergeron, P. 2006, *AJ*, 132, 1221
- Kawka, A. & Vennes, S. 2009, *A&A*, 506, L25
- Kawka, A., Vennes, S., Oswalt, T. D., Smith, J. A., & Silvestri, N. M. 2006, *ApJ*, 643, L123
- Kawka, A., Vennes, S., & Vaccaro, T. R. 2010, *A&A*, 516, L7
- Kenyon, S. J. & Garcia, M. R. 1986, *AJ*, 91, 125
- Kepler, S. O., Kleinman, S. J., Nitta, A., Koester, D., Castanheira, B. G., Giovannini, O., Costa, A. F. M., & Althaus, L. 2007, *MNRAS*, 375, 1315

- Kilic, M., Allende Prieto, C., Brown, W. R., Agüeros, M. A., Kenyon, S. J., & Camilo, F. 2010a, *ApJ*, accepted
- Kilic, M., Allende Prieto, C., Brown, W. R., & Koester, D. 2007a, *ApJ*, 660, 1451
- Kilic, M., Brown, W. R., Allende Prieto, C., Kenyon, S. J., & Panei, J. A. 2010b, *ApJ*, 716, 122
- Kilic, M., Brown, W. R., Allende Prieto, C., Pinsonneault, M., & Kenyon, S. 2007b, *ApJ*, 664, 1088
- Kilic, M., Brown, W. R., Allende Prieto, C., Swift, B., Kenyon, S. J., Liebert, J., & Agüeros, M. A. 2009, *ApJ*, 695, L92
- Kilic, M., Stanek, K. Z., & Pinsonneault, M. H. 2007c, *ApJ*, 671, 761
- Koester, D. 2008, arXiv:0812.0482
- Koester, D. & Wilken, D. 2006, *A&A*, 453, 1051
- Kulkarni, S. R. & van Kerkwijk, M. H. 2010, *ApJ*, 719, 1123
- Kurtz, M. J. & Mink, D. J. 1998, *PASP*, 110, 934
- Landau, L. D. & Lifshitz, E. M. 1958, *The classical theory of fields* (Oxford: Pergamon Press)
- Liebert, J., Bergeron, P., Eisenstein, D., Harris, H. C., Kleinman, S. J., Nitta, A., & Krzesinski, J. 2004, *ApJ*, 606, L147
- Marsh, T. R., Dhillon, V. S., & Duck, S. R. 1995, *MNRAS*, 275, 828
- Marsh, T. R., Gaensicke, B. T., Steeghs, D., Southworth, J., Koester, D., Harris, V., & Merry, L. 2010, *ApJ*, submitted
- Massey, P., Strobel, K., Barnes, J. V., & Anderson, E. 1988, *ApJ*, 328, 315
- Mullally, F., Badenes, C., Thompson, S. E., & Lupton, R. 2009, *ApJ*, 707, L51
- Munn, J. A. et al. 2004, *AJ*, 127, 3034
- Panei, J. A., Althaus, L. G., Chen, X., & Han, Z. 2007, *MNRAS*, 382, 779
- Perets, H. B. 2010, *ApJ*, submitted

Schönrich, R., Binney, J., & Dehnen, W. 2010, MNRAS, 403, 1829

Steinfadt, J. D. R., Kaplan, D. L., Shporer, A., Bildsten, L., & Howell, S. B. 2010, ApJ, 716, L146

A. DATA TABLE

Table 3 presents our radial velocity measurements. The Table columns include object name, heliocentric Julian date, heliocentric radial velocity, and velocity error.

Table 3. Radial Velocity Measurements

Object	HJD +2450000	v_{helio} (km s ⁻¹)
J0755+4906	5150.867780	393.5 ± 17.5
...	5267.639886	395.4 ± 12.6
...	5267.654862	27.8 ± 11.5
...	5267.668518	-421.8 ± 18.0
...	5268.675038	-363.5 ± 23.8
...	5268.685061	-490.9 ± 19.5
...	5268.703821	217.5 ± 22.8
...	5268.713913	384.5 ± 22.0
...	5269.617361	-358.8 ± 22.0
...	5269.628715	-386.8 ± 31.4
...	5269.661999	344.2 ± 29.2
...	5269.674290	-72.7 ± 24.7
...	5276.680582	-457.7 ± 31.1
...	5276.693521	-350.4 ± 23.8
...	5276.704122	93.0 ± 18.9
J0818+3536	5151.924119	-92.7 ± 16.2
...	5267.686783	-52.8 ± 13.9
...	5267.703298	-55.3 ± 17.7
...	5267.718598	-15.1 ± 14.4
...	5268.662172	-225.0 ± 15.4
...	5268.798134	-28.8 ± 12.4
...	5269.648138	-350.8 ± 19.7
...	5270.749626	-273.1 ± 17.5
...	5276.658219	-107.1 ± 30.6
...	5276.802073	-290.2 ± 20.7
...	5277.689765	-287.2 ± 31.7
...	5277.807903	-155.8 ± 24.1
J0923+3028	3818.669260	-22.3 ± 13.4
...	5204.841296	123.3 ± 23.6
...	5204.849317	364.1 ± 29.1
...	5204.856366	170.1 ± 21.0
...	5204.864851	-165.2 ± 23.2
...	5204.871899	-288.4 ± 20.7
...	5204.880060	-114.6 ± 18.5
...	5204.887108	101.8 ± 24.9
...	5204.897757	273.5 ± 17.7

Table 3—Continued

Object	HJD +2450000	v_{helio} (km s ⁻¹)
...	5204.904794	15.5 ± 18.6
...	5204.912596	−198.1 ± 16.4
...	5204.927423	−27.7 ± 16.8
...	5204.934460	255.0 ± 11.6
...	5204.942365	245.2 ± 21.3
...	5204.949403	49.5 ± 16.5
...	5204.957216	−293.3 ± 21.2
...	5204.964265	−248.4 ± 22.3
...	5204.972922	2.3 ± 20.3
...	5204.979960	320.7 ± 15.0
...	5204.987969	260.3 ± 21.7
...	5212.845177	171.1 ± 32.3
...	5212.858568	183.6 ± 45.1
...	5221.767105	−248.2 ± 28.5
...	5221.774790	−307.1 ± 19.1
...	5221.790045	153.6 ± 29.9
...	5221.797082	316.9 ± 35.1
...	5221.804744	85.6 ± 26.1
...	5221.811793	−170.3 ± 21.6
...	5221.819339	−318.7 ± 23.4
...	5221.826388	−189.8 ± 35.6
...	5221.834351	144.9 ± 17.4
...	5221.841400	269.2 ± 20.0
...	5221.848935	133.3 ± 13.0
...	5221.855983	−142.1 ± 15.5
...	5221.863657	−282.4 ± 12.6
...	5221.870706	−153.8 ± 18.7
...	5221.878275	162.7 ± 19.0
...	5221.885313	300.7 ± 17.0
...	5221.892859	129.4 ± 16.1
...	5221.899896	−136.3 ± 17.6
...	5221.907431	−266.4 ± 20.3
...	5221.914468	−177.7 ± 29.9
...	5221.922038	−15.5 ± 22.4
...	5221.929086	285.6 ± 18.0
J1233+1602	5268.822025	−351.5 ± 10.6

Table 3—Continued

Object	HJD +2450000	v_{helio} (km s ⁻¹)
...	5268.840648	-157.5 ± 13.1
...	5268.864607	171.2 ± 9.3
...	5268.887073	301.6 ± 15.5
...	5268.909573	147.3 ± 9.1
...	5269.793880	290.8 ± 14.6
...	5269.805316	278.4 ± 17.4
...	5269.816670	151.1 ± 15.8
...	5270.766544	-344.9 ± 14.1
...	5270.775294	-347.4 ± 20.0
...	5276.854668	97.5 ± 16.4
...	5276.866474	191.1 ± 12.1
...	5276.875895	298.3 ± 12.6
J1422+4352	4596.887690	-290.1 ± 10.9
...	5268.969670	-364.8 ± 12.5
...	5268.978929	-331.1 ± 9.8
...	5268.988397	-352.3 ± 13.6
...	5270.854102	-373.6 ± 14.8
...	5384.771754	-93.0 ± 15.4
...	5384.793095	-36.8 ± 15.6
...	5385.726490	-314.3 ± 21.4
J1439+1002	3882.885571	-8.6 ± 7.9
...	4922.892856	-21.0 ± 6.9
...	4922.892856	82.0 ± 4.5
...	4922.977535	116.4 ± 5.6
...	4923.020372	137.9 ± 18.8
...	4923.973820	-126.2 ± 7.4
...	4924.020430	-191.7 ± 18.9
...	5267.943738	-56.8 ± 14.4
...	5267.969654	-50.0 ± 11.2
...	5268.036672	-15.3 ± 25.6
...	5268.957759	111.4 ± 7.0
...	5268.962158	110.6 ± 5.1
...	5269.971779	-147.0 ± 14.4
...	5269.977266	-165.6 ± 11.1
...	5270.959442	-189.1 ± 5.7
...	5270.979860	-178.5 ± 9.1

Table 3—Continued

Object	HJD +2450000	v_{helio} (km s ⁻¹)
...	5271.011239	-119.8 ± 9.1
...	5275.934512	120.3 ± 10.2
...	5277.886834	-216.8 ± 10.5
...	5384.660342	-246.8 ± 10.3
...	5385.755771	202.7 ± 47.3
J1448+1342	4237.919202	-21.6 ± 15.6
...	5276.885957	-38.5 ± 19.0
...	5276.892265	-0.1 ± 25.0
...	5276.900298	-22.9 ± 17.6
...	5276.906641	-39.8 ± 23.6
...	5277.023591	-182.0 ± 69.6
...	5277.896227	-3.2 ± 25.8
...	5277.902686	-14.6 ± 27.1
...	5277.911552	-49.7 ± 32.8
...	5277.917988	4.5 ± 20.8
...	5277.990376	-53.4 ± 22.3
...	5277.996811	-82.0 ± 27.8
...	5278.004983	-35.8 ± 20.4
...	5278.011256	-23.8 ± 16.6
...	5384.666893	-0.3 ± 16.7
...	5384.752430	-56.4 ± 20.0
...	5385.762534	-12.3 ± 32.9
J1512+2615	3879.873052	-127.7 ± 11.2
...	5267.949987	56.7 ± 17.4
...	5267.974827	87.6 ± 19.0
...	5267.997247	49.5 ± 18.6
...	5269.017902	-96.7 ± 14.4
...	5269.023840	-101.2 ± 17.1
...	5270.006995	-74.1 ± 19.5
...	5271.002158	66.2 ± 16.6
...	5271.017749	1.0 ± 28.4
...	5271.024775	53.1 ± 26.8
...	5276.915247	42.9 ± 17.9
...	5277.013574	129.0 ± 31.5
...	5277.943822	-154.4 ± 25.1
...	5384.675640	-189.8 ± 22.7

Table 3—Continued

Object	HJD +2450000	v_{helio} (km s ⁻¹)
...	5384.763249	-127.7 ± 15.2
...	5385.747861	22.7 ± 28.1
J1630+2712	5009.892692	-239.7 ± 18.9
...	5267.958434	-47.1 ± 18.0
...	5267.983829	24.0 ± 14.3
...	5268.011944	103.0 ± 14.5
...	5269.005570	-280.4 ± 13.7
...	5269.985526	17.1 ± 15.1
...	5270.988168	-80.9 ± 14.5
...	5276.925057	-133.0 ± 19.3
...	5276.999529	-332.8 ± 29.4
...	5384.809434	-345.1 ± 15.2
...	5384.868187	-197.8 ± 31.1
...	5385.781067	126.8 ± 13.6
...	5385.842754	-58.9 ± 34.1
J2119–0018	5008.884992	-15.2 ± 18.7
...	5152.578978	7.8 ± 10.5
...	5152.591870	266.2 ± 10.8
...	5153.581786	-203.5 ± 16.9
...	5153.590153	-319.1 ± 21.7
...	5153.597282	-396.7 ± 15.3
...	5153.605372	-329.3 ± 18.1
...	5153.612500	-159.7 ± 15.1
...	5153.628726	306.2 ± 23.9
...	5153.636966	357.4 ± 17.9
...	5153.645148	312.6 ± 18.3
...	5153.654661	154.2 ± 28.5
...	5153.663884	-115.9 ± 29.2
...	5157.626210	383.6 ± 31.6
...	5157.635329	343.2 ± 16.8
...	5157.644287	265.7 ± 17.8
...	5157.653291	26.0 ± 28.6
...	5157.662260	-139.8 ± 25.8
...	5157.672131	-427.6 ± 17.2
...	5158.586060	337.8 ± 21.8
...	5158.594878	312.5 ± 16.8

Table 3—Continued

Object	HJD +2450000	v_{helio} (km s ⁻¹)
...	5158.603454	150.1 ± 30.5
...	5158.613036	-173.7 ± 25.2
...	5158.625477	-383.8 ± 17.5
...	5158.636229	-443.9 ± 18.3